Solid-Solid Reactions in Series: A Modeling and Experimental Study

A. K. Suresh and Chinmay Ghoroi
Dept. of Chemical Engineering, Indian Institute of Technology–Bombay, Powai, Mumbai 400 076, India

DOI 10.1002/aic.11829
Published online July 23, 2009 in Wiley InterScience (www.interscience.wiley.com).

Reactions among particulate solid phases are important and abundant in many materials, chemical, and metallurgical process industries. Many of these are reaction networks, and not single-step reactions as normally assumed. There is no theoretical framework available for the analysis of such systems, and single-reaction models derived from the gas–solid literature continue to be used. Formation of cement clinker in the rotary cement kiln is a prime example of the genre*, in which mechanistic aspects play an important role in determining energy efficiency and the composition and nature of the phases that form. In the present study, we formulate a model within the ambit of the ''shrinking core'' class of models, for reactions in series among solid phases. The model shows the presence of one or two moving fronts in the reacting particle, depending on the relative rates of the processes involved. A single Thiele-type parameter controls the model behavior, at once describing the relative rates of the intermediate formation and consumption processes, and the diffusion-reaction competition for the product formation step. The model has been shown to reduce to the well known single reaction models at the limits of low and high values of the Thiele parameter. Experimental data have been obtained on the calcia-alumina system, an important one in cement manufacture, in the temperature range 1150–1250°C. The model has been fitted to these data and the kinetic parameters determined. The comparison bears out the salient features of the theory, and shows that a degree of diffusion limitation exists for the intermediate conversion step under these conditions. The diffusivity values estimated are in the range of 10^{-19} to 10^{-18} m^2/s and agree with values found in the literature for similar systems. The rate constant for the intermediate conversion step is of the order of 10^{-6} s^{-1}. This being among the first such determinations, this value awaits confirmation from other studies.* © 2009 American Institute of Chemical Engineers *AIChE J,* 55: 2399–2413, 2009

Keywords: solid-solid reactions, tricalcium aluminate, reaction intermediate, kinetic model, two-step reactions, cement phase

Introduction

Solid-solid reactions are important in chemical and metallurgical process industries spanning a wide spectrum, from traditional sectors such as cement and construction materials to modern semiconductor and electrochemical materials. In spite of a long history of application, it would be fair to state that modeling efforts in this class of reactions remain far behind their counterparts in fluid-phase reactions. For example, while detailed analysis of series-parallel reaction networks for fluid phase reactions are available from even the classical literature, and the influence of contacting configuration on rate and selectivity is well worked out, one rarely sees a mention of such networks in the context of solid

Correspondence concerning this article should be addressed to A. K. Suresh at aksuresh@iitb.ac.in
Current address of Chinmay Ghoroi: Invensys Development Centre, Invensys Process System, SimSci-Esscor, Ascendas IT Park, Orion Building, Madhapur, Hyderabad, India - 500 081.

phase reactions. Yet, instances of such reaction networks abound in practical situations. Reactions in the rotary cement kiln among oxides of calcium, silicon, aliminium, and iron, not to mention other minor additives, provide a prime example. Design in such cases is often based on empirical pseudohomogeneous kinetic forms, and there exists considerable potential for optimizing reactor size and energy consumption through a better understanding of intrinsic reaction mechanisms. The present work is part of a broader study of the cement kiln reactions and focuses on model development for a case of consecutive solid-solid reactions. Experiments have been carried out on a system of importance in its own right as well as in the context of the cement industry, namely the $CaO - Al_2O_3$ system. The data have been used to test the applicability of the model to such systems in general.

With solid-solid reactions, the absence of anything like free motion in the solid lattices and the particulate nature of all the reactant species involved, result in unique and peculiar features, making their understanding with any degree of rigour extremely difficult. Although questions continue to be raised over the applicability of kinetic concepts from fluid-phase literature to explain these reactions, models based on such concepts nevertheless form the mainstay in attempts to explain their kinetic features. Thus, for the prototypical reaction,

$$\hat{\nu}_A A(s) + \hat{\nu}_B B(s) \rightarrow \hat{\nu}_p P(s), \tag{1}$$

the kinetics have been usually explained, assuming the reaction to take place in a single step, and one of the reactants (say B) to diffuse into the other (A), in terms of models of the type:

$$g(\alpha) = kt \tag{2}$$

where $g(\alpha)$ is a function of the conversion (α) of the nondiffusing reactant A. The form derives from fluid–solid reaction literature. Normally, the reaction is assumed to occur at a front which moves into the nondiffusing reactant particle with time. The choice of the diffusing component is usually justified on the basis of the activation energy values observed when the models are fitted to experimental data.[1] The form of $g(\alpha)$ depends upon the particle geometry and assumptions made on the underlying process and rate controlling mechanism. Although the form of Eq. 2 accommodates empirical formulations based on an overall reaction order also, the front-reaction hypothesis has gained ground insofar as it has something of a mechanistic basis. Although diffusion and reaction are, in general, the rate processes involved,models based on diffusion control are often more successful than others based on reaction control at the phase boundary or a mechanism of nucleation and growth. The fit of such models to data over the entire conversion range is not always satisfactory, but is often adequate and the models have continued to be applied because of the simplicity of analysis. Jander,[2] Ginstling-Brounshtein[3] and Valensi-Carter[4,5] models have been the most popular in this *genre*; other models have been listed elsewhere.[6–8]

Although alternative modeling frameworks have been developed in more recent times, these appear to have their limitations in the current state of their development. A comparative analysis of all these models has been presented recently in Ghoroi and Suresh[9] where the case for considering the reaction to take place throughout a region (as opposed to at a front) has been argued. This "volume-reaction" approach[10] accommodates front-reaction as a special case and should therefore be regarded as more general.

In many industrially important cases of the type 1, contrary to what is assumed, the reaction actually occurs through one or more intermediates, which are often sufficiently stable under the conditions of reaction as to accumulate to significant extents. The conversion of calcia (B) and alumina (A) by reaction to tricalcium aluminate (C_3A), an important reaction in cement manufacturing, is a case in point. Our earlier work on this reaction[8] has highlighted the inadequacy of models of the type 2 in interpreting data from such reactions, and the need for better models.

Although there may be a case for assuming the product formation to take place at a front (as shown in Figure 1a) in most situations involving a single reaction, the situation is likely to be different, when a reaction network is involved. Buscaglia and Milanese[11] have modeled the situation in which the immobile reactant goes through a number of intermediate phases in a series manner, considering several moving fronts demarcating zones occupied by individual intermediates (shown in Figure 1b for the case of a single intermediate, I). In their model, the flux of the diffusing reactant at any front is partly consumed at the front and partly proceeds inward to the next front, with no consumption taking place in between. However, it seems likely that, if one or more intermediates are experimentally observed to accumulate to significant concentrations, not all reactions can take

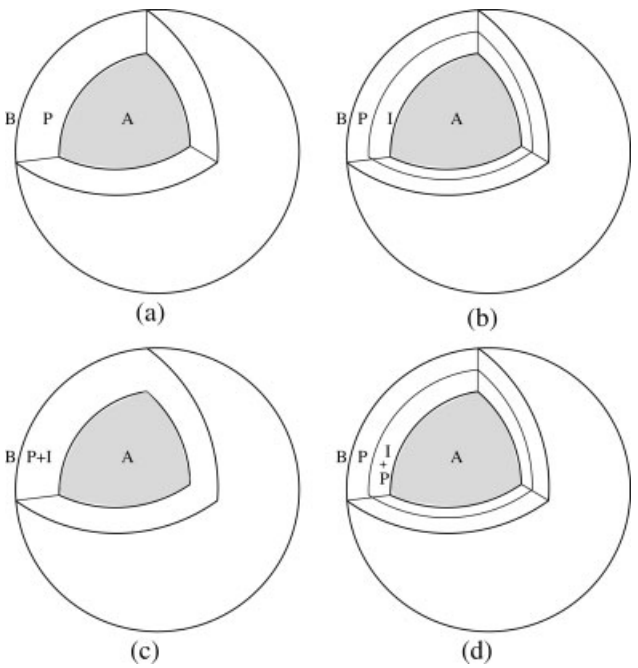

Figure 1. Schematic representation of reacting particle with different reaction fronts.

(a) Single step reaction, reaction at a front, (b) Two-step reaction, particle zones as assumed by Buscaglia and Milanese,[11] (c) Two-step reaction (initial stages): particle zones as considered in this work, (d) Two step reaction (later stages) particle zones as considered in this work.

Table 1. Different Aluminate Phases Along with Intermediate(s) in Mixed Powder Experiments

Reaction System with Mole Ratio	Intermediate(s) Reported	Final Phase	References
$3CaO:Al_2O_3$	CA_2	C_3A	Mackenzie and Hadipour[18]
$4CaCO_3:Al_2O_3:Fe_2O_3$	C_3A, $C_{12}A_7$	C_4AF	Mackenzie and Alasti[19]
$CaCO_3:Al_2O_3$	C_3A, $C_{12}A_7$, CA_2	CA	Singh and Ali[1]
$CaCO_3:Al_2O_3$	$C_{12}A_7$, C_3A	CA	Chou and Burnet[20]
$3CaO:Al_2O_3$	$C_{12}A_7$, CA	C_3A	Chou and Burnet[20]
$CaCO_3:2Al_2O_3$	CA	CA_2	Singh and Mondal[21]
$CaCO_3:Al_2O_3$	$C_{12}A_7$, CA_2	CA	Scian et al.[22]
$CaO:2Al_2O_3$	CA	CA_2	Singh et al.[23]
$CaO:Al_2O_3$	$C_{12}A_7$, C_3A, CA_2	CA_2	Singh et al.[23]
$CaCO_3:Al_2O_3$	C_3A, $C_{12}A_7$	CA	Mohamed and Sharp[24]
$3CaCO_3:Al_2O_3$	$C_{12}A_7$, CA	C_3A	Mohamed and Sharp[25]
$3CaCO_3:2Al(OH)_3$	$C_{12}A_7$, CA	C_3A	Mohamed and Sharp[25]
$3CaCO_3:2Al(OH)_3$	$C_{12}A_7$	C_3A	Ghoroi and Suresh[8]
$9CaCO_3:C_{12}A_7$	Nil	C_3A	Ghoroi and Suresh[9]

place at fronts. For example, consider a two-step series reaction. Even if the first reaction (formation of the intermediate) takes place at a front (call this front 1), as the diffusing reactant sweeps through the product region on the way to reaching this front, it should be consumed by the second reaction in the entire zone where the intermediate is present (Figure 1b,c). If the second reaction is to be considered to take place at a front (say front 2) and not in a region, front 1 would remain stationary till front 2 comes and coincides with it. Examining this scenario from the start suggests that the only case in which both reactions take place at reaction fronts is the one in which the fronts coincide, and no intermediate would then be experimentally observable. This then would not be different to considering the series reaction as a single, overall reaction which is the stoichiometric sum of the two reactions. One does not see volume reactions being considered in the solid–solid reaction literature,[9] but the preceding discussion shows that such a consideration is inevitable in the general case of consecutive reactions. In situations involving multiple reactions in series, there would exist "mixed zone(s)" within the particle which contain more than one species, their relative proportion being a function of radial position. At later stages as the intermediate gets completely consumed a pure product zone develops in the outer region. During the existence of the mixed zone, however, reaction(s) will occur throughout the zone. Indeed, in our recent work,[9] we have shown that volume reaction concepts[10] have a place even for a single reaction.

Cement clinkerization is an example of a complex system which involves numerous physico–chemical processes, including reaction networks of varying degrees of complexity. Apart from the calcination step, a typical dry process cement manufacture involves mainly solid–solid reactions where oxides like lime, alumina, silica, and iron oxide react together and form the different calcium silicate (C_3S and C_2S), calcium aluminate (mainly C_3A), and calcium alumino-ferrite (C_4AF) phases ($C \equiv CaO$, $A \equiv Al_2O_3$, $S \equiv SiO_2$ and $F \equiv Fe_2O_3$). CaO is found to be the diffusing component in these calcia – alumina and calcia – silica reaction systems.[12] Kinetics of these systems have been experimentally studied separately in pellet – pellet systems (pellets of two different pure oxides pressed together before reaction) and mixed powder reaction systems (powder mixture of appropriate amounts of different powders mixed together which are then studied in pelletized form or powder form).

It is evident from the literature on pellet-pellet experiments that several product "layers" can form between two reacting oxide pellets after heating the diffusion couple at high temperatures for sufficient time. The diffusing component diffuses through these layers to the surface of non diffusing component at the other end. Kohatsu and Brindley[13] have fired the pellet combination of CaO and corundum up to 1300°C for up to 20 days and established the sequence of product layers from the lime end to the alumina end, as CaO – C_3A – $C_{12}A_7$ – CA – CA_2 – CA_6 – Al_2O_3, with the relative thicknesses of the phases as $C_{12}A_7 > C_3A > CA > CA_2 > CA_6$. Similar studies are also reported by Weisweiler and Ahmed[14] for calcia – alumina and Ference and Maria[15] for calcia – metakaoline system. In all cases phase formation has been identified, and their sequence confirmed, by EPMA. In the case of calcia – silica system also such pellet-pellet experiments have been reported by Jander and Hoffman[16] and Weisweiler et al.[17] Several silicate phases (C_3S_2, CS, CS_2, C_3S, etc.) were identified within the reaction zone, and the thickness of the product layer (y) was found to follow a parabolic relation with reaction time:

$$y^2 = kt \tag{3}$$

Although the extent and nature of the intermediate phases is often significantly different in mixed powder experiments, the existence of appreciable amounts of intermediate phases is nevertheless seen in these cases also. Table 1 summarizes the studies on the calcia-alumina system. Thus experimental results from both the systems suggest that these reactions are complex in nature. In spite of this, phase formation in cement clinkerization is considered to be a single step reaction and front-reaction models are generally used, often ignoring the contribution of intermediate phase(s) during the kinetic calculations. The error involved in treating this type of reaction system using the conventional front-reaction models has been pointed out in our previous work on formation of tricalcium aluminate from the oxides.[8]

Apart from the complexity of the reaction system, Table 1 also illustrates the lack of consensus on the number and nature of the intermediate phases. One of the difficulties with

experimental studies in solid–solid reactions is the number of experimental factors that can influence the observed kinetics. Particle size and its distribution, degree of homogeneity of the mixture, the method used to mix the reactants are all important. The contradictory reports one sees in the literature are likely to be due to an inadequate appreciation of these factors. These matters are discussed at length in Ghoroi and Suresh[8] where, in carefully controlled experiments on CaO – Al_2O_3 reactions with good inter-particle contact, it was shown that $C_{12}A_7$ is the sole intermediate which forms on the way to the final product, C_3A.

Following our previous experimental results on C_3A, phase formation from the starting oxides can be taken as a specific instance of the general scheme shown in Eqs. 4 and 5:

$$\hat{\nu}_A A(s) + \bar{\nu}_B B(s) \rightarrow \mathbf{I}(s) \tag{4}$$

$$\mathbf{I}(s) + \nu_B B(s) \rightarrow \hat{\nu}_P P(s) \tag{5}$$

$$\text{Overall}: \hat{\nu}_A A(s) + \hat{\nu}_B B(s) \rightarrow \hat{\nu}_P P(s) \tag{6}$$

where $\hat{\nu}_B = (\bar{\nu}_B + \nu_B)$. A ($Al_2O_3$) and B (CaO) are the two reactant oxides, which react with each other and form the solid intermediate, I ($C_{12}A_7$ here, in Eq. 4), which then finally converts into the solid product, P (C_3A) by further reaction with B (Eq. 5). Depending on the relative rates, three different possibilities can be identified for such systems[26]: if either (a) the first reaction is much slower than the second, or (b) the second reaction is much slower than the first, the system can be analyzed by single-reaction models. In the first case, the intermediate would not accumulate at all and reaction (6) occurs effectively in a single step. In the second, A would be completely converted to I before I starts getting converted to P, and hence I and P would not be seen together in the same sample. However, if the two reactions occur at comparable rates (a condition that can be recognized by the presence of both I and P in the same sample), the series nature of the reaction network has to be explicitly considered. And here, for reasons elaborated on in the earlier paragraphs, the appearance of the intermediate in measurable amounts implies that the second reaction should be considered a volume reaction when the two occur together.

In this work, we have formulated a general model for such a two step reaction for single-sized solid particles. The model can be considered to fall within the framework of the "Shrinking core" class of models, but with cognizance taken of the accumulation and reaction of an intermediate. The predictions of the model have been compared with the data generated on the formation of tricalcium aluminate from the oxides of calcium and aluminium.

Reaction Modeling

Model assumptions

The following are the assumptions made in the model developed for the reaction scheme outlined in Eqs. 4–6:

(1) Particles of A, the nondiffusing component, are at all times surrounded by B, the diffusing component.

(2) Mono-size spherical particles of A are assumed to start with. The volume of the particle remains constant.

(3) The first reaction is assumed to take place at a front (where A and B meet) and to be instantaneous. The second reaction is assumed to be first order in B. For reasons elaborated above, the second reaction is assumed to take place in a region (as opposed to, at a front) containing I and P.

(4) The effective diffusivity of B through the composite product layer is constant. A quasi-steady state assumption is made with respect to diffusion of B (see Ghoroi and Suresh[9] for a discussion and justification).

Model description

The particle, according to the model, is converted in several stages as shown in Figure 2. The reaction starts at the outer surface forming I. As B diffuses through this layer, product (P) begins to form. In the initial stage (stage 1) therefore, the particle consists of an unreacted core surrounded by a "mixed zone" containing I and P (Figure 2b).

In time, the outermost surface is converted completely to P. This marks the beginning of stage 2 in which the particle has three zones—an inner unreacted core, a middle "mixed zone" and an outer "product zone" in which only diffusion (without reaction) of B occurs (Figure 2c).

At an even later time (beginning of stage 3), the core disappears and the particle again has two zones (Figure 2d)—a mixed zone inside and a product zone outside. This finally gets completely converted leaving the particle with product (Figure 2e).

It is possible, depending on the relative rates of the reactions involved, for some of the stages described above to be missing in any given case. For example, if reaction 2 (Eq. 5) is slow enough, then stage 3 directly follows stage 1 with the particle having only mixed zone for a time.

The mathematical description of the stages follows.

Stage – 1: Mixed Zone and Unreacted Core Without Any Separate Product Layer. Figure 2b shows the particle in stage 1. B diffuses through the mixed zone, reacting with I and producing P by a first order reaction. The time at which the surface layer is completely converted to P marks the end of this stage.

Considering the simultaneous diffusion and chemical reaction in the sphere, the continuity equation for component B in the mixed zone is written as

$$\frac{\mathcal{D}_e}{r^2}\frac{d}{dr}\left[r^2\frac{dC_B}{dr}\right] = \nu_B k_v C_B, \qquad r_c \le r \le R_0 \tag{7}$$

with the boundary conditions

$$r = R_0, \qquad C_B = C_{B0} \tag{8}$$

$$r = r_c, \qquad C_B = 0 \tag{9}$$

Solution gives the concentration profile of B in $r_c \le r \le R_0$ as

$$C_B = \left[\frac{R_0 C_{B0}}{r}\right]\left[\frac{\sin h[(r - r_c)(\frac{\phi_v}{R_0})]}{\sin h[(R_0 - r_c)(\frac{\phi_v}{R_0})]}\right] \tag{10}$$

where ϕ_v is a Thiele modulus,

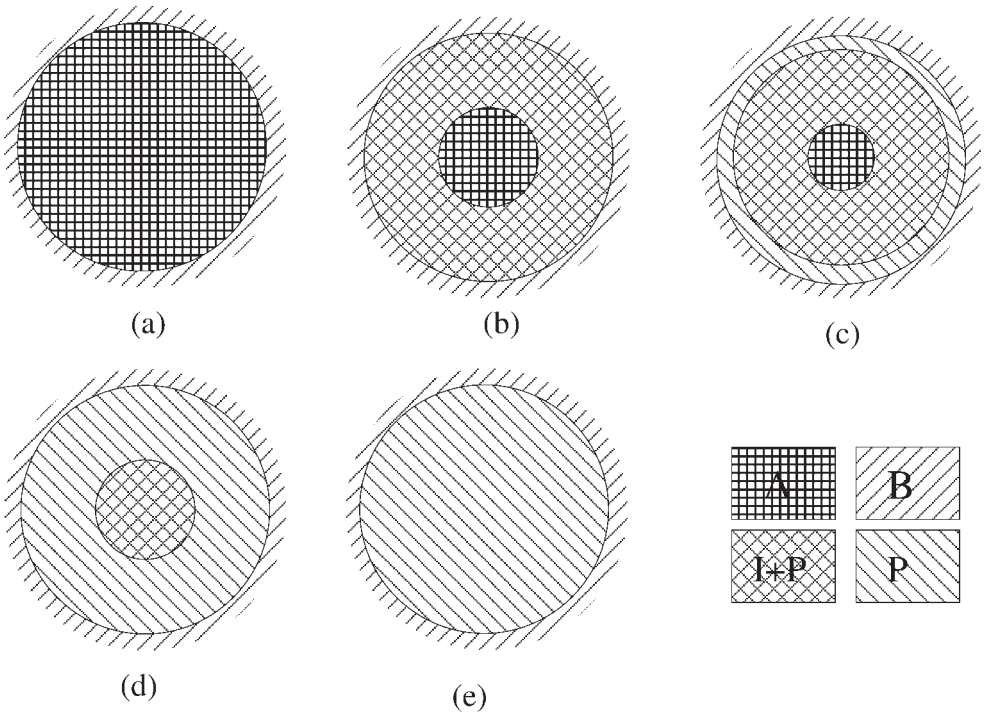

Figure 2. Reaction scheme for multilayer phase formation in spherical particle.

(a): Particle A surrounded by B, (b) Stage 1: mixed zone in annular section with a central core of A, (c) Stage 2: Pure product layer at outer periphery, followed by mixed zone and a central core of A, (d) Stage 3: Only pure product within the annular section and the central core being a mixed zone, (e): Particle completely converted into product.

$$\phi_v = \left(R_0\sqrt{\frac{v_B k_v}{\mathcal{D}_e}}\right) \tag{11}$$

The inward movement of the surface of the unreacted core can now be tracked using:

$$-\mathcal{D}_e(4\pi r^2)\left[\frac{dC_B}{dr}\right]_{r=r_c} = \frac{\bar{v}_B}{\hat{v}_A}(4\pi r_c^2)\rho_{ma}\left[\frac{dr_c}{dt}\right] \tag{12}$$

(where ρ_{ma} is the molar density of A) with the initial condition,

$$t = 0, \qquad r_c = R_0 \tag{13}$$

Solving this equation, we get the following relation between core radius and time.

$$Kt = -\phi_v + \phi_v\left(\frac{r_c}{R_0}\right)\cos h\left[(R_0 - r_c)\left(\frac{\phi_v}{R_0}\right)\right] + \sin h\left[(R_0 - r_c)\left(\frac{\phi_v}{R_0}\right)\right] \tag{14}$$

where

$$K = \left(\frac{\hat{v}_A v_B}{\bar{v}_B}\right)\frac{C_{B0}k_v}{\rho_{ma}} \tag{15}$$

It is easily verified that Eq. 10 and 14 reduce to the well known results of the classical shrinking core model with ash diffusion control, for the case of $k_v \to 0$.

Mass Balance for I. Because the reaction at r_c is assumed to be instantaneous, concentration of I at r_c is determined by stoichiometry that is,

$$C_I = \left(\frac{\rho_{ma}}{\hat{v}_A}\right) = C_{I0} \qquad \text{at } r = r_c \tag{16}$$

Conversion of I to P, at any position r, starts from the time the core passes that position, and is governed for larger times by the local rate of reaction. In other words,

$$-\frac{dC_I}{dt} = k_v C_B \qquad r_c \le r \le R_0 \tag{17}$$

with the initial condition,

$$t = t|_{r=r_c}, \qquad C_I = \left(\frac{\rho_{ma}}{\hat{v}_A}\right) \tag{18}$$

where $t|_{r=rc}$ refers to the time at which the core radius was r. Therefore,

$$C_I = \begin{cases} \left(\frac{\rho_{ma}}{\hat{v}_A}\right) - \int_{t|r=r_c}^{t} k_v C_B dt & \text{if } r_c \le r \le R_0; \\ 0 & \text{if } r < r_c \end{cases} \tag{19}$$

Applying this equation to $r = R_0$, we get the time t^* for the end of stage 1, when the reaction has consumed I completely at R_0, that is,

$$t^* = \left(\frac{\rho_{ma}}{\hat{v}_A k_v C_{B0}}\right) \tag{20}$$

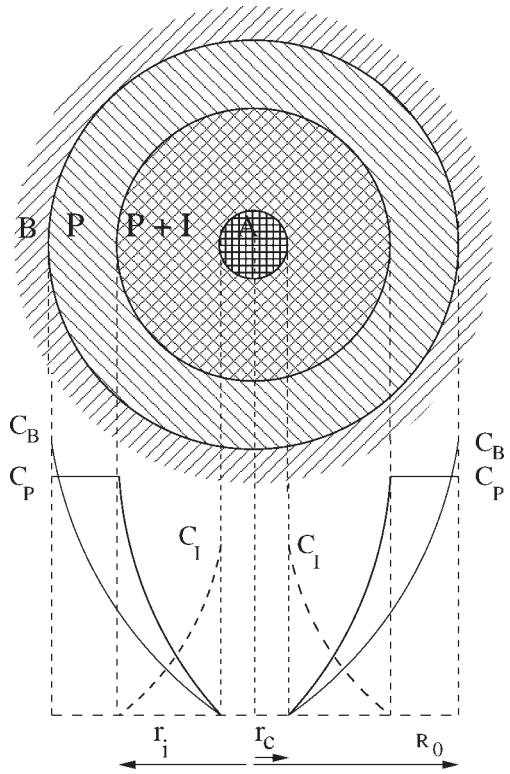

Figure 3. Schematic of partially reacted particle (stage 2) with concentration profiles.

Mass Balance for P. Rate of product formation within the mixed zone ($r_c \le r \le R_0$) can be written from considerations similar to those leading to Eq. 19, as

$$r_P = \left(\frac{dC_P}{dt}\right) = \begin{cases} \hat{v}_P k_v C_B & \text{if } r_c < r \le R_0; \\ 0 & \text{if } r \le r_c \end{cases} \tag{21}$$

with $C_P = 0$ at $t = t|_{r=r_c}$ as the initial condition.

Stage – 2. Formation of Product Zone with Mixed Zone and Unreacted Core. Beyond t^*, the mixed zone will detach from the particle surface and move inward. Figure 2c depicts this situation. Figure 3 shows the concentration profiles. A new zone will occupy the region between the mixed zone and outer surface of the particle, containing only product (product zone). The product concentration here is given by $C_{P0} = \left(\frac{\hat{v}_P}{\hat{v}_A}\right)\rho_{ma}$. The interface between product zone and mixed zone will be designated as r_i, where the concentration of the intermediate will be zero [$C_I(r_i, t) = 0$]. As there is no reaction within the product zone, the equation for B becomes

$$\frac{\mathcal{D}_e}{r^2}\frac{d}{dr}\left[r^2\frac{dC_B}{dr}\right] = \begin{cases} v_B k_v C_B & \text{if } r_c \le r < r_i; \\ 0 & \text{if } r_i \le r \le R_0 \end{cases} \tag{22}$$

with boundary conditions

$$r = R_0, \qquad C_B = C_{B0} \tag{23}$$

$$r = r_i, \qquad C_B = C_{Bi} \tag{24}$$

$$r = r_c, \qquad C_B = 0 \tag{25}$$

where C_{Bi} is the concentration of B at r_i the interface of mixed zone and product zone. Equation 22 yields two expressions for the concentration profiles of B in the two regions and we evaluate the unknown concentration at $r = r_i$ by requiring that the concentration profile as well as flux be continuous at that point. Thus we get

$$C_B = C_{B0}\left[1 - \frac{r_i(\frac{1}{r} - \frac{1}{R_0})f(r_i, r_c)}{1 + (1 - \frac{r_i}{R_0})f(r_i, r_c)}\right], \qquad r_i < r \le R_0 \tag{26}$$

$$C_B = \left[\frac{C_{Bi}r_i}{r}\right]\left[\frac{\sin h[(r - r_c)(\frac{\phi_v}{R_0})]}{\sin h[(r_i - r_c)(\frac{\phi_v}{R_0})]}\right], \qquad r_c < r < r_i \tag{27}$$

where

$$C_{Bi} = C_{B0}\left[\frac{1}{1 + (1 - \frac{r_i}{R_0})f(r_i, r_c)}\right], \qquad r = r_i \tag{28}$$

and

$$f(r_i, r_c) = \left[\frac{\phi_v r_i}{R_0 \tan h\left[(r_i - r_c)(\frac{\phi_v}{R_0})\right]} - 1\right] \tag{29}$$

Equation 12 once again governs the movement of r_c, which for this case gives

$$\left[\frac{dr_c}{dt}\right] = -\left(\frac{\hat{v}_A}{\bar{v}_B}\right)\left[\frac{\mathcal{D}_e\phi_v C_{B0} r_i}{\rho_{ma} r_c R_0}\right]\left[\frac{1}{1 + (1 - \frac{r_i}{R_0})f(r_i, r_c)}\right] \times \left[\frac{1}{\sin h\left[(r_i - r_c)(\frac{\phi_v}{R_0})\right]}\right] \tag{30}$$

The concentrations of I and P vary only in the mixed zone. In this zone they are still governed by Eqs. 19 and 21, respectively. The variation of r_i with time is obtained by requiring r_i to be the position where $C_I = 0$. Stage 2 ends when r_c arrives at the center and A is completely converted.

Stage – 3. Product Zone and Mixed Zone Without Any Unreacted Core. After the A core is completely converted the particle has once again only two zones, the product zone outside and the mixed zone inside. Figure 2d shows the particle schematically in this stage. The concentration profile of B in the mixed zone is governed by the same differential equation as before (Eq. 22) but the boundary condition at r_c (Eq. 25) is replaced by the condition

$$\frac{dC_B}{dr} = 0 \qquad \text{at } r = 0. \tag{31}$$

The analytical solutions for C_B turn out to be the same as in stage 2 with r_c set to zero.

Conversion and mass fractions

As any stage in the reaction, the conversion of A (α) and the mass fraction of product species in the particle can be calculated from the concentration profile, as follows.

Conversion of A, is given by

$$\alpha = 1 - \left(\frac{r_c}{R_0}\right)^3 \tag{32}$$

Moles of any species, i (where i = B, I, P) within the particle, given its concentration $C_i(r)$ can be calculated as

$$n_i = \int_0^{R_0} 4\pi r^2 C_i(r) dr \tag{33}$$

Moles of A remaining unconverted is given by

$$n_A = \frac{4}{3}\pi r_c^3 \rho_{ma} \tag{34}$$

Mass fraction of species, i (where i = A, B, I, P) within the particle

$$x_i = \frac{n_i M_i}{n_A M_A + \Sigma_j (n_j M_j)}, \qquad j = B, I, P \tag{35}$$

where M_j stands for the molecular weight of species j.

Nondimensionalization

For a parametric study of the model, it is convenient to render it in a nondimensional form. This may be done by defining the following nondimensional variables:

$$\Psi_B = \frac{C_B}{C_{B0}}, \Psi_P = \frac{C_P}{C_{P0}}, \Psi_I = \frac{C_I}{C_{I0}}, \Psi_{Bi} = \frac{C_{Bi}}{C_{B0}}, \varphi_{BI} = \frac{C_{B0}}{C_{I0}}, \varphi_{BP} = \frac{C_{B0}}{C_{P0}} \tag{36}$$

$$\tau = \frac{t}{t^*}, \xi = \frac{r}{R_0}, \xi_i = \frac{r_i}{R_0}, \xi_c = \frac{r_c}{R_0} \tag{37}$$

After nondimensionalization, the salient model equations for different stages become

Stage – 1.

$$\Psi_B = \frac{1}{\xi}\left[\frac{\sin h[(\xi - \xi_c)\phi_v]}{\sin h[(1 - \xi_c)\phi_v]}\right], \qquad \xi_c \le \xi \le 1 \tag{38}$$

$$\left(\frac{v_B}{\bar{v}_B}\right)\phi_v \tau = -\phi_v + \xi_c \phi_v \cos h[(1 - \xi_c)\phi_v] + \sin h[(1 - \xi_c)\phi_v] \tag{39}$$

Stage – 2.

$$\Psi_B = \left[1 - \left(\frac{\xi_i f(\xi_i, \xi_c)}{1 + (1 - \xi_i) f(\xi_i, \xi_c)}\right)\left(\frac{1 - \xi}{\xi}\right)\right], \qquad \xi_i < \xi \le 1 \tag{40}$$

$$\Psi_B = \left[\frac{\Psi_{Bi}\xi_i}{\xi}\right]\left[\frac{\sin h[(\xi - \xi_c)\phi_v]}{\sin h[(\xi_i - \xi_c)\phi_v]}\right], \qquad \xi_c < \xi < \xi_i \tag{41}$$

where

$$\Psi_{Bi} = \left[\frac{1}{1 + (1 - \xi_i) f(\xi_i, \xi_c)}\right], \qquad \xi = \xi_i \tag{42}$$

and

$$f(\xi_i, \xi_c) = \left[\frac{\phi_v \xi_i}{\tan h[(\xi_i - \xi_c)\phi_v]} - 1\right]. \tag{43}$$

The equation for the core movement is given by

$$\left[\frac{d\xi_c}{d\tau}\right] = -\left(\frac{v_B}{\bar{v}_B}\right)\left[\frac{\xi_i}{\xi_c \phi_v}\right]\left[\frac{1}{1 + (1 - \xi_i) f(\xi_i, \xi_c)}\right] \times \left[\frac{1}{\sin h[(\xi_i - \xi_c)\phi_v]}\right] \tag{44}$$

and the variation in the concentration of the intermediate, by

$$\Psi_I = 1 - \int_{\tau|_{\xi=\xi_c}}^{\tau} \Psi_B d\tau \qquad \xi_c < \xi < 1 \tag{45}$$

where $\tau|_{\xi=\xi c}$ stands for the dimensionless time at which the core radius was ξ.

Stage – 3. For stage 3 all equations of stage 2 (Eqs. 40–43) are applicable with $\xi_c = 0$.

In the dimensionless coordinates, the model behavior for a given system is seen to be governed by only one parameter (ϕ_v). It is interesting to consider the significance and role of ϕ_v in the present model. As far as the second reaction is concerned, ϕ_v has the significance (as already remarked) of a Thiele modulus which determines the severity of diffusion limitations. On the other hand, because the same diffusion rate determines the rate at which the first reaction occurs, ϕ_v also compares the consumption and formation rates of the intermediate. This dual role of ϕ_v is a peculiar feature of this formulation and shows that such situations which lead to an accumulation of the intermediate because the ratio of its formation to consumption rate is large (small ϕ_v) are also situations in which the second reaction occurs throughout the mixed zone because the diffusion limitations for the reaction are small (and conversely for large ϕ_v). This was the point made earlier in the introduction on qualitative grounds.

Solution strategy

The concentration profiles of the various species in the particle, as well as the front positions as functions of time were obtained as follows. The radial field $0 < r < R_0$ was divided into several divisions (N_{core}). At any time, profiles exist only in the mixed zone, which is determined by the instantaneous positions of one or both of r_i and r_c depending on the stage of the reaction. At each radial position in the zone, the respective concentration profiles of I (as well as P) and core radius, r_c were solved as a set of at most (N_{core} + 1) ODE's. A program was written in FORTRAN for the purpose, that used the public-domain subroutine LSODES,[27] based on the Gear's algorithm. Solution requires the use of the analytical expressions for the concentration profile of the diffusing species B, as well as the position of the outer front $r = r_i$ which separates the product zone from the mixed

zone. This front was obtained as the position at which the intermediate concentration C_I goes to zero. A fourth degree polynomial, fitted to the calculated values of C_I in the region where the latter becomes adequately small, was used to interpolate for this purpose.

The concentration profiles were integrated to obtain conversion and the mass fraction of the various species according to Eqs. 32–35, respectively, taking care to use the appropriate value of the relevant concentrations depending on the location r. The integration was carried out using the extended trapezoidal rule.[28]

Table 2. Physical Constants Used in the Simulations

Parameters	Value	Units	Reference
Molar density of CaO (C_{B0})	59.28	kmol m^{-3}	Lea[30]
Molar density of $C_{12}A_7$ (C_{I0})	1.94	kmol m^{-3}	
Molar density of Al_2O_3 (ρ_{ma})	39.11	kmol m^{-3}	
Average radius of $Al(OH)_3$ (R_0)	0.52×10^{-6}	m	–
Stoichiometric coefficients			
$\mathcal{D}_A$	7	–	–
$\bar{\nu}_B$	12	–	–
ν_B	9	–	–
$\mathcal{D}_P$	7	–	–

Experimental

Experimental studies on the reaction between CaO and Al_2O_3 to give C_3A were conducted in the temperature range of 1100–1250°C. At higher temperatures the reaction was too fast to be studied by the present methods, because the first sample itself showed very high conversions. Although the reaction requires a mole ratio CaO:Al_2O_3 of 3:2, in accordance with the model assumption of B surrounding the reacting particle at all times, experiments were conducted with an excess of CaO, with a mole ratio of 5:2.

AR grade calcium carbonate and aluminium hydroxide gel powder were procured from Sisco Research Laboratories and Loba Chemie, respectively and taken as the primary reagents in the experiments. Conditions and protocols established as being necessary for obtaining reproducible kinetics in Ghoroi and Suresh[8,9] were followed in all the experiments. Both the powders were passed through a 53 μm sieve separately and the fraction passing through was used. Based on a TG-DSC analysis of the pure components, the right amounts of both the powders were taken so as to achieve the required mole ratio of the reactants. The powder mixture was then slurried in cyclohexane to achieve intimate mixing. The slurried mixture was dried in an oven maintained at 55°C. The particle size distribution of the individual powders ($CaCO_3$ and $Al(OH)_3$) as well as the powder mixture were recorded using a GALAI CIS-1 instrument (Migdal Haemek, Israel) using methanol as the suspending medium. The dried powder mixture was then calcined at 800°C for 1 h in a tube furnace. An XRD study carried out on some of the samples confirmed the complete conversion of $CaCO_3$ as well as the absence of any other reaction products. The powder mixture was then made into pellets of 12 mm diameter, using an isostatically cold press at 300 MPa. All these protocols were in accordance with the conditions established in our earlier study.[8]

A programmable-temperature high temperature chamber furnace (60 F4, Super Kanthal Okay Electric Furnace, Bysakh, India), programmed for the desired temperature (in the temperature range of 1100–1250°C) was used to carry out the reaction in the pellets in order to obtain isothermal kinetics. The furnace was heated to the desired isothermal temperature and then the green pellets introduced. Samples were taken out after the desired time intervals, air quenched and stored in a desiccator for quantitative X-ray diffraction (QXRD) analysis.

Phase quantification was done using the Internal Standard method,[29] as described in greater detail in Ghoroi and Suresh.[8] All reacted pellets were ground using an agate mortarand-pestle, and the sample passed through the 53 μm sieve to minimize the XRD intensity variation with particle size. A fixed amount of an internal standard (rutile, 14.65%), also sieved through the 53 μm sieve, was added to the ground and sieved sample and mixed thoroughly under cyclohexane. The mixture was then dried as before and examined by Philips X'Pert PRO diffractometer using Cu as a target at a voltage of 40 kV and current of 30 mA. Randomly oriented samples were prepared for X-ray diffraction by back-loading technique to avoid any preferential orientation. Scans were taken from for a 2θ range of 5–70° with step size of 0.017° and different phases were quantified using previously prepared calibration samples. Calibration procedures and methods of interpretation of XRD results have been detailed elsewhere.[8]

Simulation Results

In our studies[9] on the conversion of $C_{12}A_7$ to C_3A, rate constant and diffusivity for that system were estimated by fitting the Ishida-Wen model to the data. For the parameters estimated in that study, ϕ_v values for the present work would lie in the range 2–15 in the temperature range 1150–1300° C. We may expect a similar range of values to fit the data of this study. To see the general behavior of the model therefore, initial simulations were carried out using $\phi_v = 4.68$ as a typical value. Table 2 gives the values of the other parameters used in the simulations.

Development of concentration profiles and reaction zones

Figure 4 shows the concentration profiles of the diffusing reactant B and the reaction intermediate I at different (dimensionless) times till the end of stage 1. For diffusion-reaction in a sphere, reaction reduces the convexity (towards the y-axis) of the solute concentration profiles, and for the chosen value of ϕ_v, the profiles are seen to be nearly linear. The profiles of I show that with time, as the core moves inward, the concentration at the surface falls, ultimately reaching zero. This marks the end of stage 1. The concentration profiles of P will be exactly complementary to those of I and are not shown.

Figure 5 shows the concentration profiles of B and I as they develop in stages 2 and 3. The profile of B is seen to become increasingly flatter in the outer part of the particle as the core moves inward. The region of pure diffusion (product zone) and that of diffusion-reaction (mixed zone) are distinguishable by the nature of the B profile in these

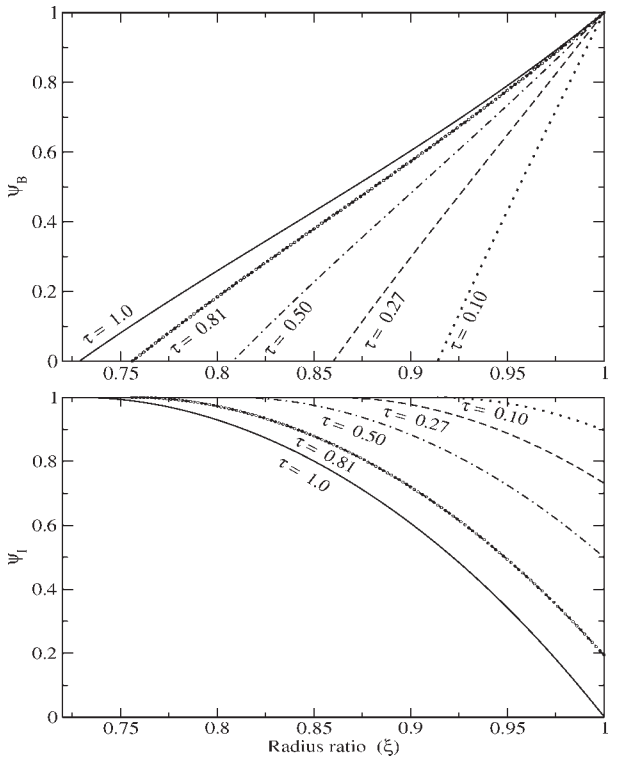

Figure 4. Concentration profiles of diffusant B (top) and intermediate I (bottom), in Stage 1 at different dimensionless times.

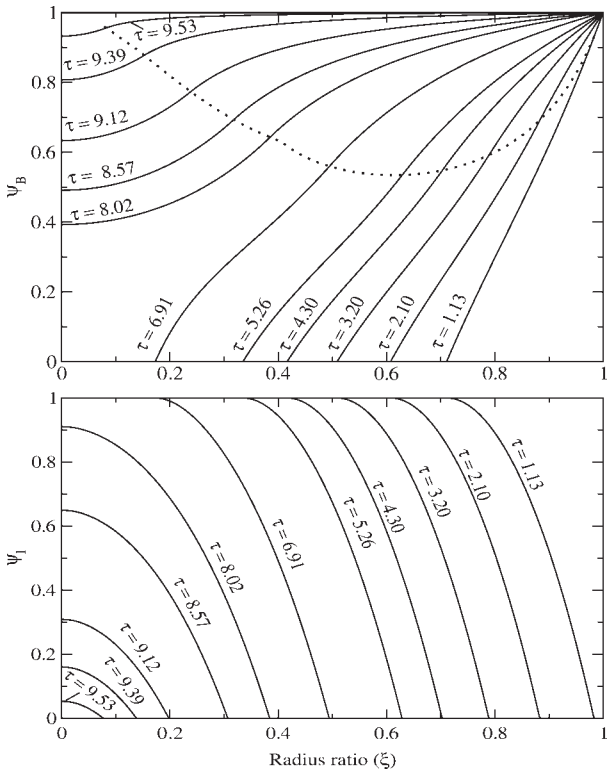

Figure 5. Concentration profiles of the diffusant B (top) and I (bottom) in stages 2 and 3, at different dimensionless times for $\phi_v = 4.68$.

The dashed line in the top figure shows the locus of ξ_i.

regions. The dashed line in the figure joins the points (ξ_i, Ψ_{Bi}) on the curves, and shows the position of the boundary ξ_i at different times. It is seen that the concentration Ψ_{Bi} at this boundary first decreases, and then increases as B penetrates deeper into the particle. The mixed zone is also recognizable in the figure showing the I profiles as the region extending between $\Psi_I = 1$ and $\Psi_I = 0$. For $\phi_v = 4.68$, the core disappears (i.e., reactant conversion reaches 1) around $\tau = 7.5$ and the particle enters into stage 3. It may be noted how the boundary condition (Eq. 31) changes the profiles in the interior after the core disappears.

The profiles of I in Figure 5 show that the thickness of mixed zone ($\xi_i - \xi_c$) (denoted by δ_{th} in what follows), remains nearly constant with time in stage 2, increasing only slightly as the particle proceeds towards stage 3. Figure 6 shows the variation of δ_{th} with time for different values of the parameter ϕ_v. The general trend, especially for $\phi_v \gg 2$, is as follows: the mixed zone initially expands (stage 1) till it detaches from the surface at $\tau = 1$, then remains nearly of constant thickness, expanding slightly as the core reaches the centre (stage 2), and finally contracts as its outer boundary ξ_i shrinks (stage 3). The case of ϕ_v being $\sim$2 (actually, 1.933 for our system) is somewhat special since, as will be shown presently, this is the smallest value of ϕ_v for which stage 2 can exist. For smaller values of ϕ_v, the core disappears before stage 1 ends ($\tau = 1$), and the particle proceeds directly into stage 3. This explains why the curves for such values of ϕ_v do not show the plateau characteristic of stage 2.

The second interesting feature of stage 2, as Figure 5 shows, is that the profiles of I are nearly self-similar. To examine this self-similarity better, the profiles of I at different times in stage 2 are plotted against a normalized distance in the mixed zone, defined as $\zeta\left(=\frac{\xi-\xi_c}{\xi_i-\xi_c}\right)$, in Figure 7. The profiles shown are for two different values of ϕ_v. The profiles, with small error, can be represented by a single curve, which interestingly, is substantially independent of ϕ_v as well. The P-profiles show similar behavior and are not discussed further. These results therefore show that in stage 2, the mixed zone moves as a block, almost without any internal changes, into the particle with time.

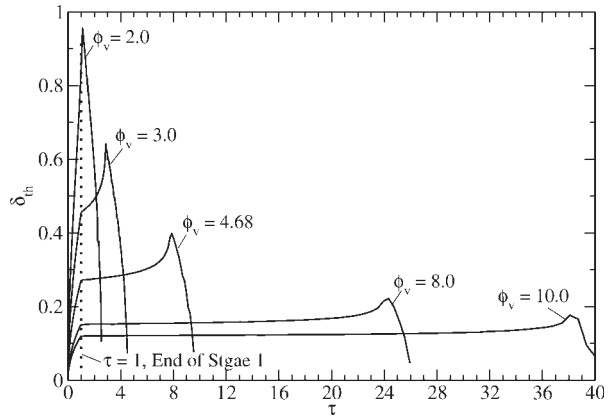

Figure 6. Thickness of the reaction layer (δ_{th}) vs. τ for different ϕ_v.

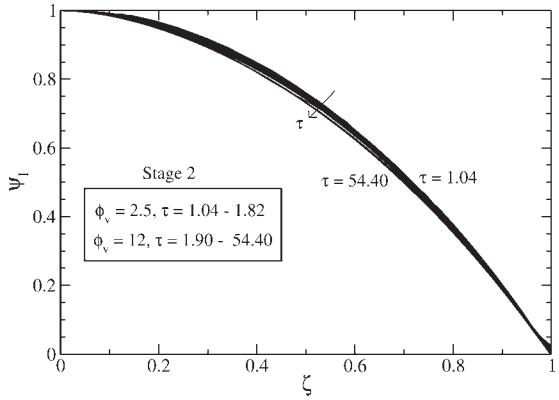

Figure 7. Concentration profiles of I in the mixed zone, plotted as a function of a normalized distance for different times.

The ranges of τ shown are different for the two cases because stage 2 extends over different time periods depending on the value of ϕ_v.

While the results so far have concerned the phenomena inside a reacting particle, Figure 8 shows the variation of conversion and mass fractions of A, B, I, and P (x_A, x_B, x_I, and x_P, respectively) with time (calculated using Eq. 35), for $\phi_v = 4.68$. Mass fraction of I first increases and then decreases to zero, showing the expected behavior of a reaction intermediate. The maximum concentration of the intermediate as well as the time for which it persists, both depend on the value of ϕ_v—the smaller the value of ϕ_v, the larger the height of the Intermediate peak, and the shorter the (dimensionless) time for which it persists. The figure also shows the mass fraction of P on a total as well as on a calcia-free basis (x'_P). The latter quantity has been often used in the literature in place of conversion,[25] in the interpretation of kinetic data. The figure shows the error in doing this when the accumulation of the intermediate is significant.

Limiting cases of the model: Comparison with single reaction models

For cases in which the second reaction is slow, the possibility of the core reaching the center of the particle before complete consumption of I at the particle surface, and hence, of the particle transiting directly from stage 1 to stage 3, was suggested earlier. Figure 9 shows the position of the core radius at the end of stage 1 ($\tau = 1$) for different values of ϕ_v, calculated from Eq. 39 for the calcia-alumina system. The corresponding conversions α are also shown. Clearly, the smaller the value of ϕ_v, the smaller the core (and the larger the α) at the end of stage 1. Substituting $\xi_c = 0$ at $\tau = 1$ in Eq. 39 allows us to solve for the value of ϕ_v ($= \phi_v^*$) below which the particle is completely converted before the end of stage 1:

$$1 + \frac{\nu_B}{\bar{\nu}_B} = \frac{\sinh \phi_v^*}{\phi_v^*} \tag{46}$$

For our system, this equation gives a value of about 1.933 for ϕ_v^*. Thus for values of ϕ_v less than 1.933, the calcia-alumina system transits from stage 1 to stage 3 directly. This limit is clearly seen in Figure 9. It would therefore be expected that, for $\phi_v \ll \phi_v^*$, the particle gets converted entirely to I (without the second reaction proceeding significantly) and only later forms P. This represents one of the two limiting cases of the two reaction system mentioned in the Introduction, in which the second reaction is sufficiently slow as not to occur to any substantial extent till the particle is completely converted by the first reaction.

Figure 9 also shows that, for large values of ϕ_v ($\phi_v \gg \phi_v^*$), the core would have hardly moved inward by the end of stage 1. Further, as Figure 6 shows, the mixed zone remains thin at all times for such large values of ϕ_v and, in the limit, can be approximated by a surface—the second reaction is so fast that the two-reaction system is equivalent to a single reaction (the stoichiometric sum) taking place at the core surface—the second reaction is so fast relative to the first that the intermediate cannot accumulate to any measurable extent.

The different stages described earlier in the section on model description can now be understood in terms of the thickness of the reaction layer (δ_{th}). In Figure 10, model simulations for three different values of ϕ_v ($\phi_v < \phi_v^*$, $\phi_v = \phi_v^*$, and $\phi_v > \phi_v^*$) are shown. Although for the case of $\phi_v > \phi_v^*$, all three stages exist, for $\phi_v \leq \phi_v^*$, clearly stage 2 is

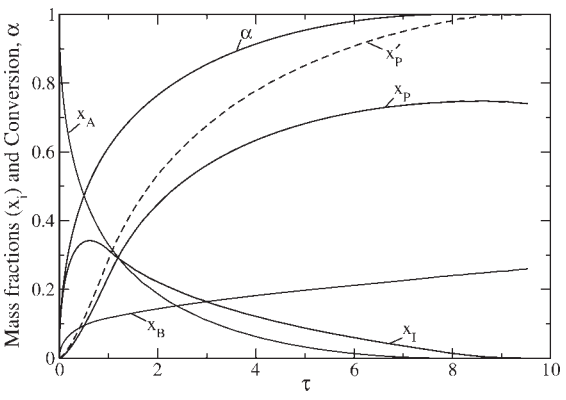

Figure 8. Mass fractions of A, B, I, and P inside the particle and conversion of A vs. τ.

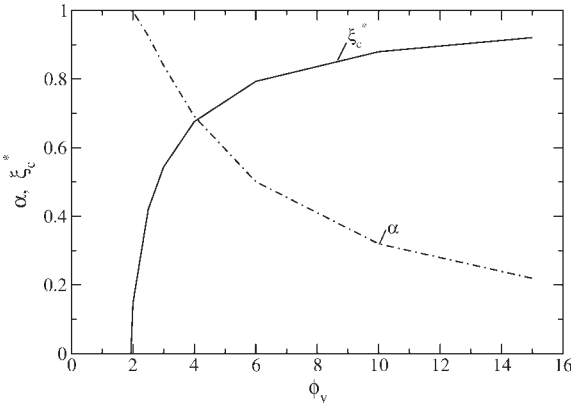

Figure 9. Core radius and conversion at the end of stage 1, for different values of ϕ_v.

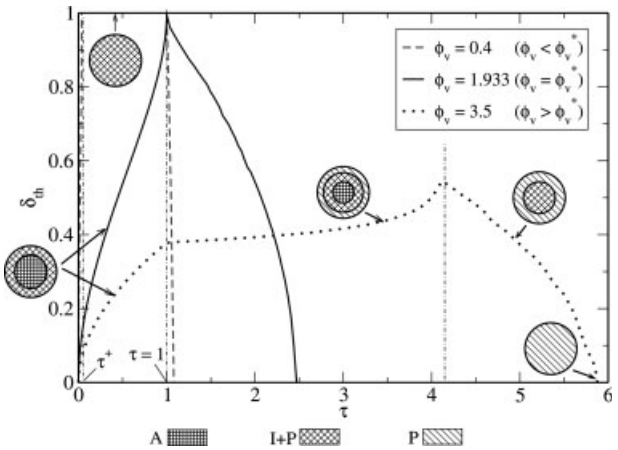

Figure 10. Reaction layer thickness vs. τ at different stages of model (at different ϕ_v).

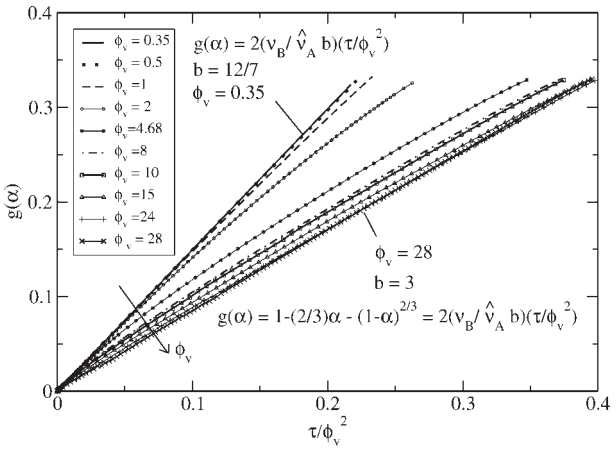

Figure 11. Plot of $g(\alpha)$ vs. $(\frac{\tau}{\phi_v^2})$ to demonstrate the limiting cases of the present seriesreaction model, in which single reaction models suffice for the conversion-time behavior.

missing (absence of a plateau) and stage 3 directly starts after stage 1.

An issue of some importance from the point of view of how such consecutive reaction systems are to be analyzed is the identification of regions in the parameter space in which simpler, single reaction models are adequate. The two limiting situations mentioned earlier can now be quantitatively considered in order to establish this.

Large ϕ_v Limit. The Ginstling-Brounstein model, which treats the case of a single reaction

$$A + bB \rightarrow \text{Product} \tag{47}$$

(A: nondiffusing reactant, B: diffusing reactant, P: Product) taking place at a moving front in a spherical particle, can be written in terms of the present variables, as

$$g(\alpha) = 1 - \frac{2}{3}\alpha - (1-\alpha)^{2/3} = 2\left(\frac{\nu_B}{\hat{\nu}_A b}\right)\left(\frac{\tau}{\phi_v^2}\right). \tag{48}$$

(It is easily shown that Eq. 48 can be derived from Eq. 39 in the limit of $\phi_v \rightarrow 0$). Thus, a plot of $g(\alpha)$ vs. $\frac{\tau}{\phi_v^2}$ would be expected to show a linear behavior independent of ϕ_v in the limit of large ϕ_v. Figure 11 shows such plots for the calcia-alumina system. The lower straight line in the figure is the line given by Eq. 48, for the stoichiometry of the overall reaction (Eq. 6, $b = 3$). The curves for different ϕ_v are seen to asymptote to this line for values of $\phi_v > 24$. This establishes the large-ϕ_v limit of the present model, in which the reaction system is equivalent to a single reaction that is their stoichiometric sum.

Small ϕ_v Limit. Equation 46 gives the limiting value ϕ_v^* of ϕ_v, below which the particle gets completely converted in stage 1 itself. Within this limit, we would further require that the conversion of I to P be negligible in the time it takes for complete conversion, so that reactions (4) and (5) may be considered to be separated in time. We may use Eq. 39 to find the dimensionless time τ^+ required for complete conversion for $\phi_v < \phi_v^*$, and Eq. 45 for calculating the intermediate concentration at the surface $\xi = 1$ at this time. These give:

$$\tau^+ = \frac{\bar{\nu}_B}{\nu_B}\left(-1 + \frac{\sinh \phi_v^*}{\phi_v}\right) \tag{49}$$

and

$$\Psi_{I1}^+ = 1 - \tau^+ \tag{50}$$

Figure 12 shows how, for the calcia-alumina system, the time required for complete conversion and the surface concentration of the intermediate at complete conversion vary with ϕ_v. For all these cases ($\phi_v < \phi_v^*$), the first reaction goes to completion well within stage 1. For values of $\phi_v < 1$, the surface concentration drops by less than 23% due to the occurrence of reaction (5) during the time the particle gets completely converted. Thus, we may consider the two reactions to be separated in time for values of $\phi \ll 1$. In this limit, we would expect that the conversion of the particle follows Eq. 48 with the stoichiometry of reaction (4). Figure 11 shows this limit also, and it is seen that the limit

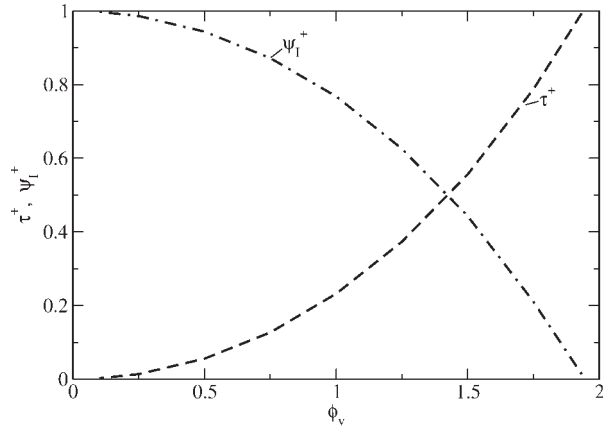

Figure 12. Dimensionless time required for complete conversion and the surface concentration of the intermediate at complete conversion as a function of ϕ_v, for cases of $\phi_v < \phi_v^*$.

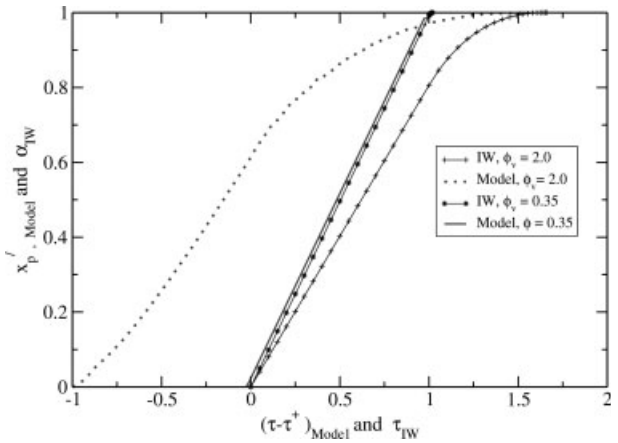

Figure 13. Comparison of the second reaction performance with that predicted by the Ishida-Wen model in the limit of small ϕ_v.

is quite well approximated by the model for values of $\phi_v < 0.5$.

Although the first reaction thus follows the Ginstling-Brounshtein kinetics in this limit, the second reaction takes place throughout the particle over longer timescales. Such a volume-reaction case for a single reaction has been modeled by Ishida and Wen,[10] who show that the particle gets converted in two stages, the first of which applies till the reactant (in this case I) is completely consumed at the surface $\xi = 1$, and the second of which applies for later times. These stages therefore correspond to the period $\tau^+ < \tau < 1$ and $\tau > 1$ (our stage 3), respectively, of the present model. Figure 13 shows a comparison between the present model and the Ishida-Wen model. The conversion of Ishida-Wen model would correspond to the product mass fraction (on a calcia-free basis) of our model. Also notice that the time is reckoned from the instant the core reaches the centre for the purpose of comparison. The agreement is seen to improve as ϕ_v decreases. In particular, for $\phi_v < 0.35$ the models are virtually indistinguishable.

Calcia-Alumina System: Parameter Estimation and Model Validation

The mean size of the individual reactant particles were comparable at 2.52 μm for $CaCO_3$ (range 0.5–12.0 μm) and 1.05 μm for $Al(OH)_3$ (range 0.5–4.0 μm). The reactant mixture had a mean size of 1.7 μm (range 0.5–6.0 μm). The other properties of interest are tabulated in Table 2.

Isothermal experiments to study the kinetics of C_3A formation from CaO and Al_2O_3 were performed at 1150°C, 1200°C, and 1250°C. A typical set of XRDs, comparing samples reacted for 1 h at different temperatures, is shown in Figure 14. Mass fractions of C_3A and $C_{12}A_7$ at different times, for each of the experimental temperatures, have been calculated from such diffractograms, using the calibration curves and shown in Figure 15. $C_{12}A_7$ peaks very early in these experiments and therefore the rising part of the curve is not captured well in the data; the general character of the curve for $C_{12}A_7$, however, shows the sequential nature of the reaction and its status as an intermediate. The increasing

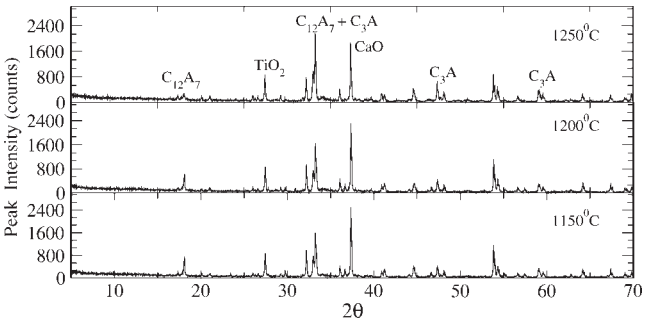

Figure 14. X-ray diffractograms of sample collected at different temperatures after 1 h of reaction.

velocity of reaction with temperature is also obvious from the figure.

It should be noted that what are measured in the experiments (and what are shown plotted in Figure 15) are the mass fractions of the intermediate and final product in the reaction mixture, and include any unreacted calcium oxide. The mass fractions in the alumina particles, on a calcia-free basis, may be calculated from these measurements by estimating the unreacted calcia from mass balance. In our earlier work,[8,9] we have compared the mass balance-based procedure with a chemical analysis of free lime and found that the two agree to within 2%. Mass fraction data on a calcia free basis, calculated in this manner, are discussed below, where they have been used for parameter estimation from the model.

The parameters of our model may be considered to be $\mathcal{D}_e$ and ϕ_v, which between them incorporate the reaction rate constant as well as diffusivity of B. Over the temperature range of interest, these parameters were estimated by a "Chi-square" procedure as was described in Ghoroi and Suresh.[9] The function to be minimized, here with respect to two parameters, is

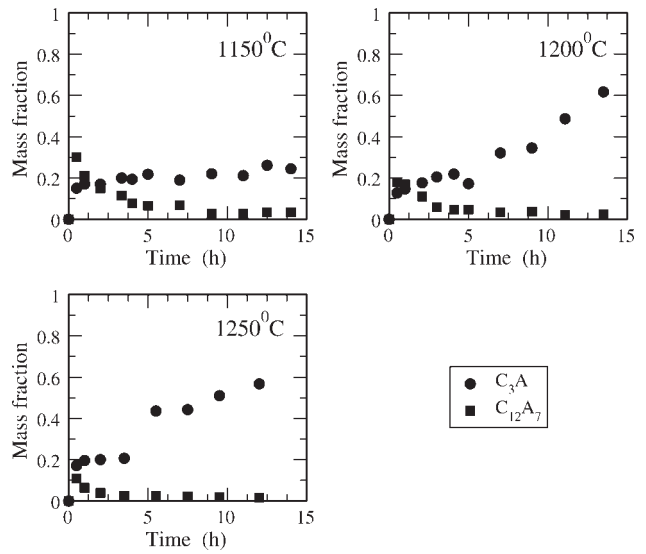

Figure 15. Mass fractions of C_3A, $C_{12}A_7$ vs. time for experiments with 5:2 $CaCO_3$ and $Al(OH)_3$.

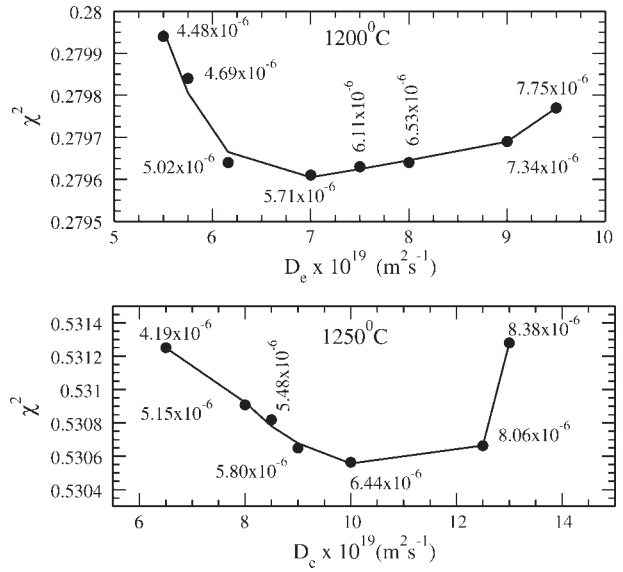

Figure 16. χ^2 vs. assumed $\mathcal{D}_e$ plot for different temperatures.

Values shown correspond to the best fit k_v for the parameter $\mathcal{D}_e$.

$$\chi^2(\mathcal{D}_e, \phi_v) = \sum_{i=1}^{N} \left[\frac{x'_I(i) - x'_I(t_i; \mathcal{D}_e, \phi_v)}{\sigma_i}\right]^2 + \sum_{i=1}^{N} \left[\frac{x'_P(i) - x'_P(t_i; \mathcal{D}_e, \phi_v)}{\sigma_i}\right]^2 \quad (51)$$

where x'_I and x'_P are the calcia free mass fractions of intermediate I and product P. One of the parameters (parameter 1, normally $\mathcal{D}_e$) was fixed (at about the value estimated for the conversion of $C_{12}A_7$ to C_3A the from earlier work[9]), and the other (parameter 2) determined by χ^2 minimization (σ_i assumed as 1). In each case, the value of the minimum χ^2 achieved was noted. The procedure was repeated for several values of parameter 1 and a plot of the minimum χ^2 vs. parameter 1 was made to locate the "global" minimum. Typical plots for two temperatures are shown in Figure 16. As the figure shows, in general, the minima were fairly broad. Although the following discussion is based on the parameter values at the global minimum in Figure 16, the uncertainty in the values because of the above factor needs to be kept in mind. The corresponding values of $\mathcal{D}_e$ and k_v are the estimates for the set.

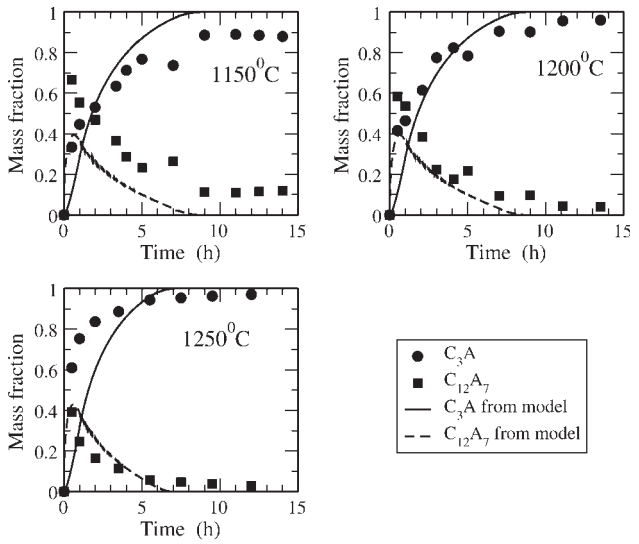

Figure 17. Fitted mass fractions (calcia free basis) of C_3A, $C_{12}A_7$ vs. time from model simulation and experiments (with 5:2 $CaCO_3$ and $Al(OH)_3$).

Table 3. Parameters Obtained from Model at Different Temperatures

Temperature (°C)	k_v (s^{-1})	$\mathcal{D}_e$ ($m^2\ s^{-1}$)
1150	4.65×10^{-6}	5.70×10^{-19}
1200	5.71×10^{-6}	7.0×10^{-19}
1250	6.44×10^{-6}	1.0×10^{-18}

In Figure 17, we compare the experimental data (on a calcia-free basis) with the model calculations for the best-fit values of the parameters, at different temperatures. Although the model captures the general trends satisfactorily at all temperatures, it is seen that the data at 1150°C seem to stop short of complete conversion, whereas for the fitted parameters, the model would predict complete conversion within the timescale of the experiment. One possibility is that the parameters need more refinement, because model calculations do show an extended tail in the conversion of the intermediate for small values of ϕ_v. With the available data, it would be difficult to speculate on any special circumstances that limit the conversion to below 100% at the lower temperatures, and it must be assumed that the rate at large times is small, not zero. Estimated k_v and $\mathcal{D}_e$ values at each temperature are given in Table 3. Figure 18 shows that the parameters follow the Arrhenius' dependence on temperature fairly well. From the plots, we recover values of 101 kJ/mol and 59 kJ/mol for the activation energies of $\mathcal{D}_e$ and k_v, respectively, although data at more temperatures would be needed

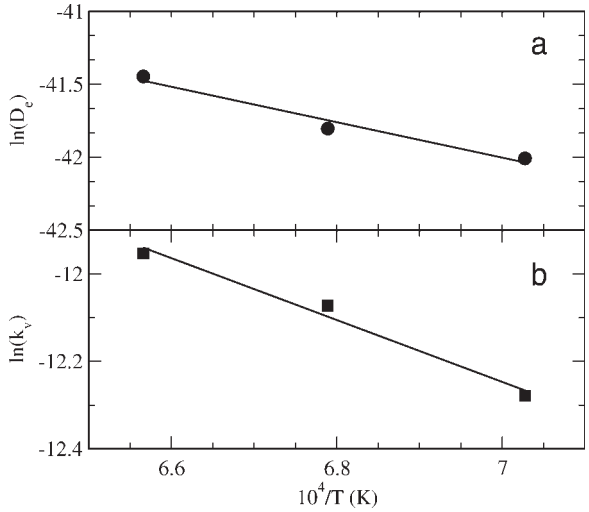

Figure 18. (a): ln($\mathcal{D}_e$) vs. (1/*T*) plot and (b): ln(k_v) vs. (1/*T*) plot as calculated from model.

to conclusively state the values of the activation energies. Such as they are, the value for $\mathcal{D}_e$ is in the range of values reported for diffusivities.[8,9] Not much data is available on the magnitude of temperature dependence of rate constants of solid-phase reactions because these processes are routinely assumed to be diffusion-limited. The one value reported by Ghoroi and Suresh[9] for activation energy for the rate constant seems much higher than found in this study. More comments on the comparison between these two studies follow.

Ghoroi and Suresh[9] estimated parameters for the conversion of $C_{12}A_7$ to C_3A using Ishida-Wen model. The reaction they studied is the second reaction of the system being studied here, and hence a comparison is possible between the two studies. However, a few differences have to be kept in mind. As Table 2 reports, the particle size available for our work is that of the precursor of alumina and not of the reacting particle itself, a fact that introduces some uncertainty in the parameter values via the definition of ϕ_v. Also, the reacting entity is different in the present case, being composed of different starting materials. Considering these factors, a good agreement is seen for the values of $\mathcal{D}_e$ over the entire temperature range. The rate constant reported by Ghoroi and Suresh[9] is a second order rate constant, which has to be converted by dividing by C_{I0} so that it can be compared with the rate constants of Table 3. When this is done and the values compared, the agreement is reasonable at 1200°C, but not so good at the other two temperatures, a fact also reflected in the different activation energies found in the two studies. Figure 17 also shows the fit to be the best at 1200°C. Data suggest that a degree of diffusion limitation exists at 1250°C. So k_v would be poorly estimated in any case. More data is required at other temperatures (covering the entire conversion range) to fix parameter values better. Ideally, one should be able to obtain the values of k_v from a single-reaction study such as that of Ghoroi and Suresh[9] and fit the data for the sequential reaction system.

Conclusions

Interplay of diffusion and intrinsic kinetics in multiple solid–solid reactions in series plays an important role in many industrial reactions. But the area of research is still in its infancy. Several single step reaction models are available and continue to be applied in literature with little justification. The reactions among several oxides in the formation of cement clinker is a prime example. In this work, a particle level kinetic model has been formulated within the ambit of the ''shrinking core'' class of models, for reactions in series among solid phases. The model shows the presence of one or two moving fronts in the reacting particle, depending on the relative rates of the processes involved. A single Thiele-type parameter (ϕ_v) controls the model behavior, at once describing the relative rates of the intermediate formation and consumption processes, and the diffusion-reaction competition for the product formation step. For small values of the parameter (in general, for $\phi_v \ll 1$), the model behaves as two single reactions one following after the completion of the other, while for large values (in general, for $\phi_v \gg 1$), the intermediate is converted as soon as it forms so that one has only the overall reaction in effect. The stoichiometry of a given system establishes these limits, so that in any given case, the region of the parameter space in which the series nature of the reaction has to be explicitly considered, is known a priori. This knowledge can also be utilized in controlling the accumulation of the intermediate through the particle size of the reactants.

Experiments carried out on CaO – Al_2O_3 system in presence of excess CaO, bear out the general behavior predicted by the model. The model has been fitted to the data using regression procedures and yields parameter values in reasonable agreement with other data in the literature. The data show that, under the conditions of experimentation, a degree of diffusion limitation exists for the second step, so that the intermediate does accumulate to significant extents even as the final product is formed.

Acknowledgments

One of the authors (CG) was supported for a large part of this work through a project funded by the Council of Scientific and Industrial Research (CSIR), Govt. of India.

Notation

A, B = solid reactants
C_i = molar concentration of i^{th} phase at any radial position of particle A, kmol m^{-3}
C_{i0} = molar concentration of i^{th} phase at particle surface or at core, where it is maximum, kmol m^{-3}
$\mathcal{D}_e$ = effective diffusivity of B through composite product layer, m^2 s^{-1}
I = intermediate
k = reaction rate parameter, s^{-1}
k_v = reaction rate constant (volume reaction), s^{-1}
M_i = Molecular weight of i^{th} component, kg $kmol^{-1}$
N_{core} = number of core
n_i = moles of i^{th} component
r = radius, m
R_0 = initial radius of particle A, m
t = time, s
$t_{0.5}$ = time in at which conversion is 50%, s
t^* = time to complete stage 1, s
P = product P formed after reaction between I and B
x_i = mass fraction of component i
x_i' = mass fraction of component i excluding B within the particle A

Greek letters

α = fractional conversion
$\overline{\nu},\nu,\hat{\nu}$ = stoichiometric coefficients
δ_{th} = nondimensional reaction layer thickness
ϕ_v = Thiele modulus
ϕ_v^* = limiting value of Thiele modulus below which particle is completely converted before the end of stage 1
Ψ_i^* = dimensionless concentration, $= \frac{C_i}{C_{i0}}$
Ψ_I^+ = dimensionless concentration of I at particle surface at time τ^+
ρ = molar density, kmol m^{-3}
σ_i = standard deviation of i^{th} data point
τ = dimensionless time, $(= \frac{t}{t^*})$
τ^+ = dimensionless time at complete conversion ($\alpha = 1$) for $\phi_v < \phi_v^*$
ξ = radius ratio at any time, $(= \frac{r}{R_0})$
ξ_i = radius ratio at the end of product zone and starting point of mixed zone
ζ = nondimensional radial coordinate, $\left(= \frac{\xi - \xi_c}{\xi_i - \xi_c}\right)$

Subscripts

B = reactant B
B0 = B at outer surface of I
c = core

I_0 = I at initial period
mc = molar concentration

Literature Cited

1. Singh VK, Ali MM. Formation kinetics of high alumina cement phases: I-Monocalcium aluminate. *Trans J Br Ceram Soc*. 1980;79:112–114.
2. Jander W. Reaction in the solid state at high temperatures. I. Rate of reaction for an endothermic change. *Z Anorg Allgen Chem*. 1927;163:1–30.
3. Ginstling AM, Brownshtein BL. Concerning the diffusion kinetics of reactions in spherical particles. *J Appl Chem USSR (English translation)*. 1950;23:1327–1338.
4. Carter RE. Kinetic model for solid state reaction. *J Chem Phys*. 1961;34:2010–2015.
5. Carter RE. Addendum: kinetic model for solid state reaction. *J Chem Phys*. 1961;35:1137–1138.
6. Sharp JH, Brindley GW, Achar BNN. Numerical data for some commonly used solid state reaction equations. *J Am Ceram Soc*. 1966;49:379–382.
7. Doraiswami LK, Sharma MM. *Heterogeneous Reactions: Analysis, Examples and ReActor Design (v.2)*. New York: John Wiley, 1984.
8. Ghoroi C, Suresh AK. Solid-solid reaction kinetics - Formation of tricalcium aluminate. *AIChE J*. 2007;53:502–513.
9. Ghoroi C, Suresh AK. Intermediate conversion kinetics in tricalcium aluminate formation. *AIChE J*. 2007;53:2399–2410.
10. Ishida M, Wen CY. Comparison of kinetic and diffusional models for solid-gas reactions. *AIChE J*. 1968;14:311–317.
11. Buscaglia V, Milanese C. Diffusion controlled solid-state reactions of spherical particles, a general model for multiphase binary systems. *J Phys Chem B*. 2005;109:18475–18482.
12. Hao YJ, Tanaka T. Role of contact points between particles on the reactivity of solids. *Can J Chem Eng*. 1988;66:761–766.
13. Kohatsu I, Brindley GW. Solid state reactions between calcium oxide and α aluminium oxide. *Z Phys Chem*. 1968;60:79–89.
14. Weisweiler W, Ahmed SJ. Kinetics of solid state reactions in the system calcium aluminium oxide. *Zement-Kalk-Gips*. 1980;33:84–89.
15. Ference DT, Maria F. Solid state diffusion of calcium into kaolinite and illite. *Cement Concrete Res*. 1971;1:423–436.
16. Jander W, Hoffman E. Reaction in solid state at higher temperature:XI. The reaction between calcium oxide and silicon oxide. *Z Anorg Allgen Chem*. 1934;218:211–223.
17. Weisweiler W, Osen E, Eck J, Hofer H. Kinetic studies in the $CaO - SiO_2$ system, Part-I: mechanism and kinetic data of the reaction between CaO and SiO_2 powder compacts. *Cement Concrete Res*. 1986;16:283–295.
18. Mackenzie KJD, Hadipour N. Formation kinetics of Portland Cement clinker phases: III-β Dicalcium silicate and Tricalcium silicate. *Trans J Br Ceram Soc*. 1978;77:168–172.
19. Mackenzie KJD, Alasti H. Formation kinetics of Portland Cement clinker phases: II-Tetracalcium Aluminoferrite. *Trans J Br Ceram Soc*. 1978;77:162–167.
20. Chou KS, Burnet G. Formation of calcium aluminates in the lime-sinter process, Part-II: Kinetic study. *Cement Concrete Res*. 1981; 11:167–174.
21. Singh VK, Mondal UK. Kinetic Study of the thermal synthesis of calcium dialuminate above 1400°C. *Trans J Br Ceram Soc*. 1982; 81:112–113.
22. Scian AN, Porto Lo'pez JM, Pereira E. High Alumina Cements. Study of $CaO.Al_2O_3$ formation. II: Kinetics. *Cement Concrete Res*. 1987;17:525–531.
23. Singh VK, Ali MM, Mandal UK. Formation kinetics of calcium aluminates. *J Am Ceram Soc*. 1990;73:872–876.
24. Mohamed BM, Sharp JH. Kinetics and mechanism of formation of monocalcium aluminate, $CaAl_2O_4$. *J Mater Chem*. 1997;7:1595–1599.
25. Mohamed BM, Sharp JH. Kinetics and mechanism of formation of tricalcium aluminate, $Ca_3Al_2O_6$. *Thermochim Acta*. 2002;338:105–114.
26. Suresh AK. Thermal analysis in the investigation of multi-step reactive process - Applications and some issues In: *Proceedings of the fifteenth National Symposium on Thermal Analysis*, Jaipur, India: 2006:40–46.
27. Krishnan R, Alan CH. Description and Use of LSODE, the Livermore Solver for Ordinary Differential Equations. In: *Lawrence Livermore National Laboratory Report*. UCRL ID 113855 NASA Refernce Pulication 1327, 1993.
28. Press WH, Teukolsky SA, Vetterling WT, Flannery BP. *Numerical Recipes in FORTRAN: the Art of Scientific Computing*, 2nd ed. Cambridge University Press, 1992.
29. Chung HF, Smith DK. *Industrial Applications of X-ray Diffraction*. New York: Marcel Dekker, 2000.
30. Lea FM. *The Chemistry of Cement and Concrete*. Glasgow: Edward Arnold (Publishers) Ltd., 1970.

Manuscript received Aug. 21, 2008, revision received Jan. 3, 2009, and final revision received Jan. 7, 2009.